AFRL-ML-WP-TP-2007-438

PROCESSING, MICROSTRUCTURE, AND TENSILE PROPERTIES OF THE Ti-6Al-4V-1.55B EUTECTIC ALLOY (PREPRINT)

Orest Ivasishin, Roman V. Teliovych, Volodymyr G. Ivanchenko, Seshacharyulu Tamirisakandala, and Daniel B. Miracle

FEBRUARY 2007

Approved for public release; distribution unlimited.

STINFO COPY

MATERIALS AND MANUFACTURING DIRECTORATE
AIR FORCE RESEARCH LABORATORY
AIR FORCE MATERIEL COMMAND
WRIGHT-PATTERSON AIR FORCE BASE, OH 45433-7750

REPORT DOCUMENTATION PAGE

Form Approved
OMB No. 0704-0188

1. REPORT DATE *(DD-MM-YY)*	2. REPORT TYPE	3. DATES COVERED *(From - To)*
February 2007	Journal Article Preprint	

4. TITLE AND SUBTITLE
PROCESSING, MICROSTRUCTURE, AND TENSILE PROPERTIES OF THE Ti-6Al-4V-1.55B EUTECTIC ALLOY (PREPRINT)

5a. CONTRACT NUMBER
In-house

5b. GRANT NUMBER

5c. PROGRAM ELEMENT NUMBER
62102F

6. AUTHOR(S)
Orest Ivasishin, Roman V. Teliovych, and Volodymyr G. Ivanchenko (Institute for Metal Physics)
Seshacharyulu Tamirisakandala (Ohio University)
Daniel B. Miracle (AFRL/MLLMD)

5d. PROJECT NUMBER
4347

5e. TASK NUMBER
RG

5f. WORK UNIT NUMBER
M02R4000

7. PERFORMING ORGANIZATION NAME(S) AND ADDRESS(ES)
Institute for Metal Physics
Kiev, Ukraine

Ohio University
Dept. of Mechanical Engineering
Athens, OH 45701

Metals Branch/Metals Development Team (AFRL/MLLMD)
Metals, Ceramics & Nondestructive Evaluation Division
Materials and Manufacturing Directorate
Air Force Research Laboratory, Air Force Materiel Command
Wright-Patterson Air Force Base, OH 45433-7750

8. PERFORMING ORGANIZATION REPORT NUMBER
AFRL-ML-WP-TP-2007-438

9. SPONSORING/MONITORING AGENCY NAME(S) AND ADDRESS(ES)
Materials and Manufacturing Directorate
Air Force Research Laboratory
Air Force Materiel Command
Wright-Patterson AFB, OH 45433-7750

10. SPONSORING/MONITORING AGENCY ACRONYM(S)
AFRL-ML-WP

11. SPONSORING/MONITORING AGENCY REPORT NUMBER(S)
AFRL-ML-WP-TP-2007-438

12. DISTRIBUTION/AVAILABILITY STATEMENT
Approved for public release; distribution unlimited.

13. SUPPLEMENTARY NOTES
Journal article submitted to Metallurgical and Materials Transactions A.
The U.S. Government is joint author of this work and has the right to use, modify, reproduce, release, perform, display, or disclose the work. PAO Case Number: AFRL/WS 07-0565, 14 Mar 2007. This paper contains color content.

14. ABSTRACT
Boron addition to conventional titanium (Ti) alloys instigates precipitation of intermetallic TiB whiskers that provide significant increases in strength and stiffness. The eutectic composition is the maximum boron concentration that provides these benefits via melt processing while maintaining reasonable ductility and damage tolerance. The eutectic point for the most widely used Ti alloy, Ti-6Al-4V (weight percent), modified by B addition, was determined to occur at 1.55+0.05B and 1545+5 ºC. The microstructure, texture, and tensile properties of the eutectic alloy are sensitive to ingot solidification conditions and melt pool morphology. Several microstructural forms in the as-cast condition as well as their transformation during thermomechanical processing (TMP) were identified. Two types of eutectic structures, aligned and random, were obtained. Cast microstructures with random eutectic colony orientation had no marked crystallographic texture, while cast aligned microstructure had a strong [020] texture for the TiB phase and a <110> circular texture for the alpha-Ti phase.

15. SUBJECT TERMS
Ti Alloy, tensile properties, eutectic alloy, metals processing

16. SECURITY CLASSIFICATION OF:			17. LIMITATION OF ABSTRACT:	18. NUMBER OF PAGES	19a. NAME OF RESPONSIBLE PERSON (Monitor)
a. REPORT	b. ABSTRACT	c. THIS PAGE			Jonathan Spowart
Unclassified	Unclassified	Unclassified	SAR	46	19b. TELEPHONE NUMBER *(Include Area Code)* N/A

Standard Form 298 (Rev. 8-98)
Prescribed by ANSI Std. Z39-18

Processing, Microstructure, Texture, and Tensile Properties of the Ti-6Al-4V–1.55B Eutectic Alloy

OREST M. IVASISHIN, ROMAN V. TELIOVYCH, VOLODYMYR G. IVANCHENKO, SESHACHARYULU TAMIRISAKANDALA, and DANIEL B. MIRACLE

ABSTRACT

Boron (B) addition to conventional titanium (Ti) alloys instigates precipitation of intermetallic TiB whiskers that provide significant increases in strength and stiffness. The eutectic composition is the maximum boron concentration that provides these benefits via melt processing while maintaining reasonable ductility and damage tolerance. The eutectic point for the most widely used Ti alloy, Ti-6Al-4V (weight percent), modified with B, was determined to occur at 1.55±0.05B and 1545±5°C. The microstructure, texture, and tensile properties of the eutectic alloy are sensitive to ingot solidification conditions and melt pool morphology. Several microstructural forms in the as-cast condition as well as their transformation during thermo-mechanical processing (TMP) were identified. Two types of eutectic structures, aligned and random, were obtained. Cast microstructures with random eutectic colony orientation had no marked crystallographic texture, while cast aligned microstructure had a strong [020] texture for the TiB phase and a <110> circular texture for the α-Ti phase. As-cast microstructure could be significantly modified via TMP. Fragmentation of TiB occurred during 3D forging and aligned microstructures were produced after rolling or extrusion. An attractive balance of strength and ductility was obtained after solution treatment in the full β condition followed by aging. The microstructure of the Ti-6Al-4V-1.55B eutectic alloy can be controlled to tailor the property combinations.

Orest M. Ivasishin, Associate Director, Roman V. Teliovych, Head, Laboratory of Heat Treatment of Steels and Titanium Alloys, Volodymyr G. Ivanchenko, Head, Department of Phase Equilibria, are with Institute for Metal Physics, Kiev, Ukraine. Seshacharyulu Tamirisakandala, Research Assistant Professor, is with the Department of Mechanical Engineering, Ohio University, Athens, OH 45701, USA. Contact e-mail: sesh.tamirisa@dayton.net. Daniel B. Miracle, Senior Scientist, is with the Air Force Research Laboratory, Materials and Manufacturing Directorate, Wright-Patterson AFB, OH 45433, USA.

I. INTRODUCTION

Structurally efficient materials provide a direct path for reducing mass via substitutions with thinner and lighter components, thus improving performance and affordability. The requirement for higher structural efficiency (a combination of specific stiffness and specific strength) provides motivation for the development of titanium (Ti) materials and processes for aerospace applications. Boron (B) is the most efficient stiffener of Ti alloys, and addition of 0.5B gives the same modulus improvement as 6.5Al (all compositions are in weight percent) [1]. The modulus increase is due to the stiff, strong TiB phase that precipitates *in situ* upon B addition. TiB is thermodynamically and thermally stable in Ti-rich alloys, so that mechanical property improvements derived from TiB are not expected to degrade with extended exposure at elevated temperatures. Other advantages of the TiB phase in Ti alloy are that its coefficient of thermal expansion matches that of Ti so that residual stresses are not generated due to thermal cycling, and the density of TiB is essentially equal to that of Ti, which eliminates segregation during casting and does not cause weight increase penalty.

Boron is completely soluble in the liquid phase of Ti but has negligible solid solubility in the high temperature *bcc* β and low temperature *hcp* α Ti phases [2]. The intermetallic TiB phase forms via the eutectic reaction L→β+TiB as shown in the Ti-rich end of the binary Ti-B phase diagram [3], Fig. 1. Boron-modified Ti alloys, denoted generally as Ti-B alloys, can thus be classified as hypoeutectic, eutectic, or hypereutectic [4]. Increasing the B content increases strength and stiffness due to a higher volume fraction of TiB. The ductility and fracture toughness of the base alloy is retained for hypo-eutectic Ti-B alloys [5], but the ductility decreases in hypereutectic Ti-B alloys as a result of fracture that initiates at large, primary TiB particles that grow unconstrained in the L+TiB phase field to sizes as large as 100–500 μm [6]. Therefore, hypoeutectic alloys with B concentration as close to the eutectic composition as possible are of specific interest for fracture-critical applications, since they allow for maximal structural efficiency without sacrificing fracture related properties. An additional advantage of

eutectic Ti-B alloys is the ability to produce aligned or unidirectionally grown *in-situ* Ti-TiB structures by controlling solidification conditions. An important characteristic of such unidirectionally grown eutectics is their thermal stability and long-term high temperature strength, which is well documented for several eutectic alloys [7]. Mechanical properties of eutectic alloys are strongly influenced by the microstructures obtained from casting. Eutectic microstructures are governed by the temperature gradient at the solidification front, which, in turn, depends on the cooling rate. Data on the influence of these parameters for Ti-B eutectic alloys are currently unavailable.

Ingot casting may produce TiB whisker orientations that vary with position in the ingot. Directional heat flow near the mold walls may produce aligned TiB whiskers, while a random orientation can result at the ingot center. Thermo-mechanical processing (TMP) may thus be required not only to convert ingot shape, but also to control TiB morphology and orientation. The as-cast TiB whiskers can be broken up via TMP, which can retain strength and stiffness while providing isotropy by randomly orienting the TiB whisker fragments. TMP in the β phase field allows reasonably easy plastic flow and facilitates rigid body rotation of intermetallic TiB causing alignment along the direction of flow [8]. TMP parameters that influence these microstructural changes include deformation temperature, strain rate, and deformation scheme. Microstructural modification of as-cast Ti-alloy grain structure is also important, where Ti alloys exhibit Widmanstätten lath-type microstructure of the α-Ti phase with thin layers of β-Ti between the α laths. Such microstructure can be transformed into either equiaxed or lamellar type via TMP, depending on whether the processing temperature is below or above the β transus (α+β→β transformation temperature). Systematic evaluation of the effect of TMP parameters on microstructural evolution in Ti-B alloys is necessary to establish the relationship between microstructure and properties.

The eutectic reaction point (composition and temperature) is of fundamental importance to understanding and controlling the microstructure and properties of this new class of Ti-B alloys.

Although established experimentally as Ti-1.67±0.25B and 1540°C [3] for the binary system (Fig. 1), the eutectic point can shift significantly for more complex alloys. There is no experimental data for the eutectic reaction point in conventional Ti alloys modified with B, including the most widely used Ti alloy, Ti-6Al-4V (Ti64). Thermodynamic databases are generally inadequate in the composition ranges of interest to calculate this reaction with certainty. The present work is thus aimed at establishing the eutectic reaction in the Ti64-B pseudo-binary system. The evolution of as-cast microstructure and the crystallographic texture are systematically studied for a wide range of solidification conditions. The effect of B additions on the β transus is studied and the response of cast eutectic microstructure to TMP is established. Tensile properties of the Ti64-B eutectic alloy are evaluated in various microstructural conditions.

II. EXPERIMENTAL PROCEDURES

A. *Materials Preparation*

Three different Ti64-B ingot sizes were prepared. Button melts (~30 g weight) of Ti64 containing various B levels were made in a laboratory vacuum arc furnace. These buttons were used to precisely determine the composition and invariant temperature of the Ti64-B eutectic reaction. Medium-sized ingots (30 mm diameter and 150 mm length) were prepared in selected compositions via induction skull melting using a water-cooled segmented copper crucible. The charge was incrementally added to give chemical homogeneity throughout the ingot. These ingots were used to study the influence of cooling rate and temperature gradient on homogeneity of the eutectic microstructure. Large ingots (70 mm diameter) of the eutectic composition were prepared via vacuum arc-induction remelting (Fig. 2). A consumable electrode was fabricated by connecting several medium-sized ingots with threaded joints. The large ingot length could be varied by changing the number of medium-sized ingots in the electrode. A special melting unit combining traditional arc melting with induction coils was used. Independent control of power

sources for the arc (W_1) and induction coils (W_2), along with a controlled withdrawal rate (R), allowed control of the melt pool size and shape, and to thus control the temperature gradient and crystallization rate. Two combinations of parameters were used, W_1=9 kWA, W_2=40 kWA, R=0.05 mm s^{-1} and W_1=6 kWA, W_2=50 kWA, R=0.03 mm s^{-1}.

The starting materials for all melts were Ti sponge TG-100 (HB=93) (FSU standard specification) and Al60V40 master alloy. Boron was added as coarse powders of TiB or AlB_2, which were synthesized by reactive sintering of powder mixtures of elemental amorphous B with TiH_2 or Al. TiB powder synthesized by using TiH_2 was easy to crush and quickly dissolved in the liquid melt due to highly porous morphology. Chemical compositions of the materials used in this study are provided in Table 1. All the ingots possessed oxygen contents of ≤0.13 which is typical of extra-low interstitial (ELI) grade Ti64.

B. *Differential Thermal Analysis*

Differential thermal analysis (DTA) was used to precisely determine the eutectic point in the Ti64-B system. Various Ti64-B alloys were melted in yttria crucibles in a DTA chamber and subsequently solidified using controlled cooling rates in the range 0.2−2.7 K s^{-1}. DTA was also used to determine the β transus of Ti64-B alloys. A crucible-less setup was used for the β transus determination to eliminate chemical interaction with the crucible as well as to increase the DTA sensitivity. Cylindrical samples of 8 mm diameter and 10 mm length were used and a wire W/W-20Re thermocouple in direct contact with the sample was used to record temperature. Sample heating and cooling were performed at a rate of 40 K s^{-1}.

C. *Thermo-mechanical Processing*

Large-size cast ingot (70 mm diameter) of the Ti64-B eutectic was skin machined and subjected to a forging plus rolling TMP schedule is shown schematically in Fig. 3. First, the round ingot was β forged at 1100°C in three-dimensions (3D) to produce a cube 80-mm side. The cube was subsequently 1-D forged, again in the β phase field, into a slab of

130×100×20 mm^3. The slab was cut into 100×20×20 mm^3 bars and subjected to unidirectional rolling in the α+β phase field at 960°C to produce 12 mm diameter bars. In another experiment performed to determine the influence of deformation path on microstructure evolution, as-cast ingot of 30 mm diameter was directly rolled in the β phase field to produce 12 mm diameter bar. An as-cast ingot (70 mm diameter and 150 mm length) was also directly extruded in the β phase field at 1100°C using an extrusion ratio of 8.5:1 and a ram speed of 6.35 mm s^{-1}.

D. *Microstructure and Texture Evaluation*

Materials in the as-cast and wrought conditions were characterized with optical microscopy and SEM. Specimens were etched with Kroll's reagent (5 ml HF+3 ml HNO_3 + 990 ml distilled H_2O). Deep etching for 30 minutes was performed on selected samples to evaluate the TiB morphology and orientation. X-ray characterization was done using CuK_α radiation. Coupled θ–2θ texture analysis techniques were used to determine crystallographic orientations. The distribution of elements in individual phases was studied using electron probe microanalysis.

E. *Tensile Testing*

Tensile tests were performed on the as-cast and wrought conditions at room temperature per ASTM E8 standard. Round dog-bone specimens of 20 mm gage length and 4 mm gage diameter were used. Tests were conducted on an Instron 3367 machine at a constant cross-head speed corresponding to an initial strain rate 10^{-4} s^{-1}. At least three tests were performed on each condition and average values are reported. Fracture surfaces were examined in SEM to understand the deformation and damage mechanisms**.** Dynamic elastic modulii were determined by measuring ultrasonic wave velocity in both the longitudinal and transverse directions.

III. RESULTS AND DISCUSSION

A. *Eutectic Point in Ti64-B System*

Thermodynamic calculations using PANDAT software predict an eutectic point of Ti64-1.4B and 1594°C for the Ti64-B system (Fig. 4a). For Ti64 containing 0.18O (typical oxygen level in

commercial grade), the predicted eutectic point shifted to Ti64-1.65B and 1650°C (Fig. 4b). Calculations using ThermoCalc [9] predict an eutectic point of Ti64-1.58B and 1597°C for the Ti64-B system (Fig. 4c). All predictions show a narrow L+β+TiB three-phase field above the eutectic solidus. The databases supporting each of these calculations have only limited experimental validation in the composition ranges of interest, and therefore uncertainty exists with the accuracy of these predictions.

Experimental studies [10][11] showed that alloying Ti with 6Al does not change the eutectic B content but increases the eutectic temperature by 30°C relative to the binary system, while addition of 4.5V to Ti decreases the eutectic temperature by 20°C [12]. Using these results, a simple additive approach gives an estimated eutectic temperature of 1551+10°C, which is noticeably lower than thermodynamic predictions. In order to establish the eutectic transformation in Ti64-B system precisely, buttons with B concentrations in the range 1.4−1.67 were prepared via arc melting (Table 1). The Ti64-1.4B alloy microstructure, Fig. 5a, contains dendritic primary β phase, confirming that this composition is hypoeutectic. In the Ti64-1.67B alloy, primary TiB particles (Fig. 5b) show that this concentration is hypereutectic. The primary TiB are often hollow with hexagonal cross-section.

Ti64 alloys containing 1.5, 1.55, and 1.6 B were analyzed using DTA, and the cooling curves are presented in Fig. 6. Each curve broadly shows two major thermal events, one near 1500°C representing solidification and one near 900°C representing the β→α transformation. The cooling curve for Ti64-1.5B exhibits two superimposed thermal events associated with solidification (Fig. 6a). The first event initiates at 1552°C and corresponds to primary β solidification, while the second event at 1535°C corresponds to the eutectic transformation,

$$L \rightarrow \beta_{pr} + L_e \rightarrow \beta_{pr} + (\beta + \mathrm{TiB})_e \qquad (1)$$

where the subscript *pr* refers to primary and *e* refers to eutectic. The Ti64-1.6B cooling curve also exhibits two solidification thermal events (Fig. 6c), the first corresponding to solidification of primary TiB and the second corresponding to the eutectic reaction**,**

$$L \rightarrow \mathrm{TiB}_{pr} + L_e \rightarrow \mathrm{TiB}_{pr} + (\beta + \mathrm{TiB})_e \quad (2)$$

The cooling curve for Ti64-1.55B exhibited a single solidification thermal event that initiates at 1545°C (Fig. 6b), representing solidification through the eutectic point, $L_e \rightarrow (\beta+\mathrm{TiB})_e$. Therefore, the eutectic point occurs at Ti64-1.55±0.05B and 1545±5°C, taking into account the accuracy of DTA. This experimentally determined eutectic concentration is close to predictions by the thermodynamic approach, but the eutectic temperature differs significantly. Crystal lattice parameters measured in Ti64–1.55B for the α-Ti, β-Ti and TiB phases are: a_α = 0.2940 nm; c_α = 0.4669 nm; a_{TiB} = 0.6120 nm; b_{TiB} = 0.3061 nm; c_{TiB} = 0.4560 nm; a_β = 0.3294 nm.

B. *Microstructural Evolution in As-cast Ti64-1.55B Eutectic*

To understand the evolution of eutectic microstructure as a function of cooling rate, the eutectic alloy Ti64-1.55B was reheated above the melting temperature (to 1560°C) in a DTA and cooled at controlled rates of 0.2, 0.7, 1.3, and 2.7 K s^{-1}. At the lowest cooling rate, a regular colony-type arrangement of eutectic TiB was not found (Fig. 7a). Instead, randomly oriented TiB of various morphologies were present, including rods up to 20 μm in diameter with aspect ratios up to 10, plates of 2−4 μm thickness and aspect ratios up to 200, and coarse flakes. The high aspect ratios of TiB are due to strong anisotropy in growth rate, with the fastest growth in the [010] axial direction of rods and the long dimension of plates. The morphology and orientation of these features were confirmed through deep-etching. Such eutectic structures are generally referred to as a "coarse conglomerate of phases or degenerated eutectic" [13][14], in which each phase nucleates separately. Increasing the cooling rate gives a more regular colony-type eutectic morphology (Figs. 7b−7d). Although, a colony microstructure coexists with a degenerated eutectic in alloy cooled at 0.7 K s^{-1} (Fig. 7b), a completely colony-type eutectic prevailed with mostly plate-like TiB at 1.3 and 2.7 K s^{-1} (Fig. 7c, 7d). A colony size up to 2 mm was measured for these intermediate cooling rates. Colonies elongated in the axial direction of TiB and a reduction in colony size, to 1 mm length and 0.5 mm width for 2.7 K s^{-1}, was observed with increasing cooling rate. Much higher cooling rates (>50 K s^{-1}) were achieved by solidification in

a laboratory arc furnace, and typical eutectic microstructures obtained for these cooling rates are shown in Fig. 7e. At these higher cooling rates, TiB particles have mixed plate-like and rod-like morphologies and are combined into colonies of low regularity. Some of the rod-shaped TiB have hexagonal cross-sections and are filled with Ti alloy at the core. Microprobe analysis revealed that the alloy composition of the core of these faceted rods is roughly the same as outside the rods. Quite often, the colonies have a fan-like structure suggesting divergent, and perhaps coupled, TiB whisker growth from a common region in the sample. Some of the TiB plates or rods branch off in directions that are nearly orthogonal to the major axis of the TiB particle.

Cooling rates higher than $100\ \mathrm{K\ s^{-1}}$ were achieved near the water-cooled wall of the segmented copper crucible. The regular eutectic arrangement was destroyed and an irregular distribution of fine TiB was observed at these high cooling rates (Fig. 7f). Although the TiB morphology and distribution in this microstructure are similar to the degenerated eutectic produced at the lowest cooling rate (Fig. 7a), the higher cooling rate gives about an order magnitude reduction in the microstructural size scale. A fine, irregular eutectic microstructure defined as a "fine conglomerate of phases" forms through gas atomization [15] when solidification occurs with a large undercooling that favors a high nucleation rate. Such high cooling rates are not experienced during ingot processing in the bulk of even small ingots but are likely to occur in the thin layer close to the surface in water-cooled crucibles. Thus, the regularity, morphology, and size of TiB in the Ti64-1.55B eutectic alloy are quite sensitive to cooling rate. It is likely that a variety of microstructures may be produced in larger ingots, where variations in the cooling rate and in the direction of temperature gradients occur.

The 70 mm diameter ingot displayed a spectrum of eutectic morphologies in the billet cross-section, reflecting a range of cooling rates. A thin region (Zone 1, Fig. 8a) extends to about 6 mm inward from the water cooled crucible wall. Within Zone 1, an eutectic microstructure with random orientation of fine TiB particles closest to the mold wall transitions through an

intermediate microstructure (Fig. 8b) to a regular eutectic microstructure with TiB (both plate and rod type) aligned normal to the water cooled crucible wall (Fig. 8c). Eutectic grain boundaries could not be clearly distinguished in Zone 1. The second microstructural region (Zone 2) extends inward from Zone 1 and has a thickness of about 20 mm. Zone 2 consists of eutectic grains within which the TiB are well aligned, but the directionality changes from grain to grain (Fig. 8d, 8e). This microstructural form is produced in the region where the temperature gradients are dictated not only by heat extraction through the crucible, but also by heat extracted by the solid ingot below the melt pool (Fig. 2a). The cooling rate in this zone is expected to be of the order of a few tens of degrees Celsius per second (compare Fig. 8d with Fig. 7e). Zone 2 gradually transitions into a "degenerated" eutectic microstructure in the central region of the ingot (Zone 3, Fig. 8f, 8g). In addition to random eutectic grains, these microstructures contain coarser (mostly rod-type) TiB surrounded by TiB-free regions. The volume fraction of degenerated eutectic increases towards the ingot centerline, which indicates that low cooling rate plays a significant role in its formation (compare Fig. 8f with Fig. 7a).

A possible explanation for formation of a degenerated eutectic microstructure considers that coarser TiB rods are located between eutectic grains. Recalescence from the growing eutectic colonies may drastically reduce undercooling before colony impingement, favoring coarser TiB formation at the boundaries. An alternate explanation is that coarser TiB forms first, scavenging B from the immediately surrounding liquid, while the remaining liquid solidifies as regular colonies. In the second explanation, the coarse TiB are not to be considered as primary TiB in hypereutectic alloys since primary TiB solidification reduces the B concentration in the liquid from hypereutectic to the eutectic composition, so that eutectic zones should directly contact the TiB, rather than leaving a TiB-free zone. In either of these two explanations, such TiB are coarser than in eutectic grains and they can have an impact on the final microstructure after TMP, as shown in the next section.

Alignment of TiB occurs on a macroscopic level at moderate cooling rates (Fig. 7). This alignment can be controlled by controlling the temperature gradient during solidification. Arc remelting of a consumable electrode favors a gradient broadly in the direction parallel to the ingot axis, since the heat source is above the melt while cooling is provided by heat transfer into the solidified ingot below. However, the melt pool shape is generally non-planar, as illustrated schematically in Fig. 2a, so that the thermal gradient across the solidification front is similarly non-planar, producing microstructural directionality that depends on position in the ingot. The melt pool shape and thermal gradient can be can be controlled with an inductor, producing a more uniformly directed microstructure (Fig. 2b). Alignment of the structure is also favored by a lower solidification rate, which is accomplished by slower withdrawal of the ingot through the induction coils. On the other hand, a high solidification rate and low temperature gradient assist in formation of a random microstructure. Thus, changing the melting/solidification parameters affects both micro- and macrostructure. Two types of microstructures, aligned and random, were produced in the present work (Fig. 9). In the aligned microstructure, TiB could be more or less unidirectionally oriented in the whole ingot (Fig. 9a), while in the random case, the TiB is aligned in individual eutectic colonies, but the colonies are randomly oriented in the ingot (Fig. 9b). The Ti64 microconstituent generally displayed a transformed β lamellar morphology. The length of the individual lamellae was limited by the TiB-free spacing rather than by the β grain size, as in conventional Ti alloys. Therefore, non-uniformity in TiB distribution produced non-uniformity in the Ti64 microstructure.

C. *Texture of As-cast Ti64-1.55B*

As-cast Ti64-1.55B eutectic with random TiB microstructure did not exhibit crystallographic texture, while the aligned TiB microstructure exhibited clear evidence of texture in both TiB and α-Ti phases (Fig. 10). The TiB texture was characterized by the [020] direction oriented along the ingot axis, and the α phase exhibited a <110> circular texture. Since α forms by the transformation β→β+α according to the Burgers orientation relationships (OR) $\{001\}_\beta \| \{0001\}_\alpha$

and $<111>_{\beta} \| <1120>_{\alpha}$, the α texture should result from the β texture. The TiB and β phases form during eutectic solidification, and two possibilities exist: either each microconstituent independently chooses its own orientation and the OR in the eutectic microstructure results from those orientations, or only one phase nucleates independently and the second phase nucleates preferentially on that phase so that the texture of the latter phase depends upon the texture of the former. Reliable experimental data was measured for the TiB phase, but the β texture is difficult to measure because of the low β volume fraction in the transformed microstructure at room temperature. The β phase forms a sharp axial <100> texture upon crystallization of Ti64 [16]. If it is assumed that the same β texture is produced during solidification of the Ti64-1.55B eutectic alloy, then the measured α texture can be rationalized. A circular α texture is predicted if it is assumed that only 4 variants of the Burgers OR exists (Fig. 11a). However, approximately the same circular α texture is predicted if the <111> direction of the β phase is oriented along the ingot axis and the number of crystallographic orientations in the β→ α transformation is limited to 3 (Fig. 11b). More detailed description of the crystallization texture in Ti64-1.55B will be given after obtaining direct data on texture of β phase using high-temperature X-ray diffraction experiments [17], which are currently in progress.

D. *Beta Transus*

The β transus is the most important material parameter for the TMP of Ti alloys, since microstructural evolution sensitively depends on whether the alloy is processed above or below this temperature [18]. The β transus of Ti64 lies in the range 975−1010^{o}C, depending on the interstitial O content. The lower temperatures in this range correspond to ELI grade Ti64, while the higher temperatures relate to conventional O levels in Ti64. Thermodynamic calculations predict a β transus of 990°C for commercial grade Ti64 (Fig. 4b), well within this range. The most detailed investigation of the β transus of Ti64-B was done on pre-alloyed powder metallurgy material, which possessed supersaturated (non-equilibrium) B and low O [19]. The supersaturated B increased the β transus by about 60^{o}C relative to ELI Ti64. A lower β transus of

935°C was measured in cast Ti64-B alloys that contained around 0.1O [20], so that a range of ±60°C relative to the β transus of ELI Ti64 has been measured previously in Ti64-B alloys with low O. In the present work, DTA heating curves for Ti64 with 0.5B, 1.55B, and 1.65B are shown in Fig. 12. The β transus determined from these curves is in the range 1005–1020°C, which indicates an increase by 30–50°C compared to ELI Ti64. The β transus of boron-free Ti64 determined using similar DTA conditions was 1006°C. Additional experiments revealed that heating rate used in the DTA measurements also affects the β transus. Heating curves for Ti64-1.4B at heating rates of 20 Ks^{-1} and 80 Ks^{-1} are shown in Fig. 13, which indicate an increase in the transus by 30°C for the higher heating rate. The β transus measured on as-cast Ti64-1.55B was in the range of 1015−1020°C and the same transus was measured on samples after TMP. Considering the errors in the β transus determination using DTA, it is concluded that addition of B does not significantly alter the β transus of ELI Ti64.

A small change in the β transus may result from a change in Ti, Al, and V concentrations of the alloy microconstituents with increasing B. Formation of TiB consumes Ti, leading to corresponding increases in Al and V concentrations in the α and β phases. This increase can be partially compensated if Al and V are soluble in TiB. Microprobe measurements on coarse TiB revealed an average V content of 3.3%, while Al was hardly detectable (<0.02%). These values were used to calculate the Al and V concentrations in the metallic microconstituent as a function of B content (Fig. 14a). These predicted concentrations remain within the specification for Ti64 and are in reasonable agreement with microprobe measurements. These compositions were used to predict the shift in the β transus employing the empirical rules that 1Al increases the transus by 16.7°C while 1V decreases it by 9.1°C [21]. Predicted as well as experimentally determined β transus values are plotted as a function of B concentration in Fig. 14b. Predictions are in acceptable agreement with the measured values.

E. *Microstructural Evolution after Thermo-mechanical Processing*

The microstructure of Ti64-1.55B after 3D β forging indicates that many of the high aspect ratio TiB whiskers have fragmented during forging (Fig. 15a). Rigid body rotation of fragmented TiB occurred along the flow lines creating "wavy" paths. During subsequent 1-D β forging, partial alignment of TiB fragments normal to the forging direction occurred (Fig. 15b). The process of TiB fragmentation and alignment continued during 1-D α+β rolling in the final TMP step (Fig. 15c). Non-uniformity in TiB distribution of the as-cast microstructure, which is most pronounced in the degenerated eutectic (Fig. 8f, 8g), remained after forging (Fig 15a, 15b) and 1-D rolling (Fig. 15c) although the non-uniformity in distribution appears less pronounced due to reduction in TiB size and inter-particle spacing after TMP.

The microstructure of Ti64-1.55B after direct 1-D rolling in the β field of 30 mm diameter ingot (Fig. 16a) shows less TiB fragmentation and alignment compared to that obtained after forging plus α+β rolling (Fig. 15c). TiB particles aligned close to the rolling direction did not undergo fragmentation. Coaxial TiB fragmentation was often observed, resulting from a circular distribution of stresses around the TiB without a visible separation of fragments along their axes. TiB in other colony orientations, on the other hand, severely fractured into short fragments. Plate-like TiB fragmented to a greater extent than needle-like TiB, producing irregular platelets. Heavily faulted or fragmented TiB in the as-cast condition is likely to be responsible for this behavior (Fig. 16b). Direct extrusion of as-cast Ti64-1.55B in the β field gives an intermediate degree of TiB fragmentation and aligns a majority of the TiB along the extrusion direction (Fig. 17). These results demonstrate that the morphology, size, distribution, and orientation of eutectic TiB can be altered significantly by TMP.

F. *Tensile Properties of Ti64-1.55B*

The Ti64-1.55B alloy provides increases in stiffness of at least 15% and increases in yield and ultimate strengths of 20% relative to Ti64. Although the as-cast condition is brittle, TMP

refines microstructural features and tensile elongations up to 6% were obtained. Additional details of the mechanical properties are provided below.

Elastic Modulus

In the as-cast condition, the Young's modulus of the Ti64-1.55B eutectic with random TiB orientations is 134 GPa in both the longitudinal and transverse directions relative to the ingot axis, and the 3D forged condition also possessed a similar modulus (132 GPa) (Table 2). A simple iso-strain rule of mixtures prediction taking moduli of 110 GPa for Ti64 [18], 482 GPa for TiB [22] and ~8 vol.% TiB yields a value of 140 GPa for Ti64-1.55B, in reasonable agreement with measurements. Similar values have been reported in the literature from experiments and theoretical predictions on other Ti64-B materials [9][23][24].

Alignment of TiB increases the modulus in the longitudinal direction as a result of more efficient load transfer, but introduces elastic anisotropy. As cast microstructure with aligned TiB had a modulus of 138 GPa in the longitudinal direction and 127 GPa in the transverse direction. An additional small increase in the longitudinal stiffness, to 142–148 GPa, is observed after rolling. Anisotropy in Young's modulus can arise not only from TiB alignment, but also from crystallographic texture of the α and β phases. This additional texture can alter the level of anisotropy [24], but there is presently insufficient data to assess this effect. The effect of texture on elastic modulus is expected to be even more pronounced after TMP due to evolution of strong deformation textures as compared to the solidification texture.

Ductility

As-cast material with randomly oriented TiB is brittle, and fracture always occurred in the linear elastic range. Fracture predominantly occurs due to premature damage of the coarse plate-like TiB oriented transverse to the loading direction (Fig. 18a, 18b). In the as-cast material with aligned TiB, a small amount of plasticity was recorded with a total elongation of ~1%, and fractographs show ductile dimples (Fig. 18c) although premature failure of coarse plate-like TiB

initiated and controlled the fracture event. These observations indicate that alignment of TiB provides an opportunity to slightly improve the ductility of as-cast material. TMP improved the ductility by refining the cast microstructure and reducing the mean TiB size and inter-particle spacing. The total elongation of Ti64-1.55B increased to ~3% after 3D forging, to ~6% after 1-D rolling, and to ~5% after extrusion (Table 2). Fractography of samples in the forged condition (Fig. 19a, 19b) revealed mixed features showing areas of ductile fracture neighboring faceted areas corresponding to brittle fracture. In the rolled condition, cup and cone ductile fracture prevailed (Fig. 19c, 19d). TiB particles are often observed at the bottom of the ductile dimples indicating that plastic deformation is localized due to the presence of TiB.

Strength

The Ti64-1.55B alloy provided increases in yield and ultimate tensile strengths of about 20% relative to Ti64 [25] with similar processing history (Table 2). The strength of Ti64-1.55B that was directly rolled in the β field from as cast billet is higher than material that was cast, 3D forged and then rolled. It has been shown [26] that for slightly hypereutectic Ti64-1.7B produced by powder metallurgy that the majority of the strengthening is provided by a load-sharing mechanism due to high modulus and strength of TiB. Microstructural refinement was also found to contribute to the strengthening. In broad agreement with this result, the strengths obtained in the present work depend on the starting morphology of TiB, mode of deformation, amount of reduction, deformation scheme, and microstructural length scale.

Beta solution treatment plus aging (β-STA) after rolling increased the strength significantly compared to wrought Ti64 in the standard STA condition, which is done just below the β transus (Table 2). The high strength is attributed not only to load-sharing by TiB but also to strengthening of Ti64 by transformation of equiaxed or lamellar α+β microstructure into acicular martensite that is additionally strengthened by fine precipitates upon aging. Conventional Ti64 and similar α+β titanium alloys are typically solution treated within the α+β phase field and quenched, which leaves the primary α phase unstrengthened. Beta solution treatment is not

generally used because of rapid grain growth that causes a reduction in ductility. In the case of Ti64-1.55B, grain growth is restricted by TiB via Zener pinning and therefore allows solution treatment in the full β condition without experiencing a loss in ductility. There are not many methods by which fully β transformed fine-grained microstructures can be produced in α+β Ti alloys. The most widely studied technique is rapidly heating above the β transus with a powerful source for a short time thus preventing β grain growth [27]. Another technique is via grain boundary pinning by fine insoluble precipitates in cast materials or by fine pores in powder metallurgy processing [27]. Addition of B thus offers the potential to fundamentally alter the TMP sequences and the heat treatment of Ti alloys, with significant impact on mechanical properties.

IV. SUMMARY AND CONCLUSIONS

Ingots of Ti-6Al-4V (Ti64) alloy modified with boron were prepared by melt processing to establish the Ti64-B pseudo-binary eutectic point and to explore the relationships between processing, microstructure, and mechanical properties of the Ti64-1.55B eutectic alloy. Evolution of microstructure and texture in the eutectic alloy was evaluated as a function of ingot size, cooling rate, and temperature gradient. Response of the eutectic microstructure to thermo-mechanical processing was determined. Tensile properties were measured in various microstructural conditions. The following major conclusions are drawn from this study:

1. The eutectic composition in the pseudo-binary Ti64-B system was measured at 1.55±0.05 weight percent B and the eutectic temperature is 1545±5°C. The eutectic temperature is the same as for the Ti-B binary system, while the eutectic concentration is lowered from ~1.7 weight percent B in the binary.

2. The β transus of the eutectic Ti64-1.55B alloy is essentially unchanged from that of Ti64 due to negligible solid solubility of B in the Ti alloy and to offsetting contributions to the β transus by Al enrichment and V depletion in the α and β phases.

3. The TiB intermetallic phase scavenges Ti and V from the alloy, leading to a slight enrichment in Al and V in the metallic microconstituent, which nevertheless remains within specifications for Ti64.

4. Cooling rate had a significant influence on the morphology, size, and orientation of the eutectic TiB microconstituent. Cooling rates in the range 0.7 to <50 K s^{-1} lead to regular colony-type eutectic microstructures with a colony width in the range of 0.5-2 mm. Slow (0.2 K s^{-1}) as well as fast (>50 K s^{-1}) cooling rates resulted in an irregular or degenerated eutectic with a mixture of rod, flake, and plate TiB morphologies.

5. A combination of arc and induction power sources were used to control the melt pool morphology and hence orientation of thermal gradients. Two types of eutectic structures, aligned and random, were obtained in this way.

6. Cast microstructures with random eutectic colony orientations had no marked crystallographic texture, while cast aligned microstructures had a strong [020] texture for the TiB phase and a <110> circular texture for the α-Ti phase.

7. As-cast eutectic microstructures could be significantly modified via thermo-mechanical processing (TMP). TiB fragmentation occurred during 3D forging, rolling and extrusion. Rolling and extrusion processes aligned TiB along the working direction.

8. The moduli and strengths of Ti64-1.55B are ~20% higher than for Ti64 under similar processing conditions. As-cast material was brittle, but TMP significantly improved the tensile ductility to ~6% as a result of microstructural refinement and alignment of TiB.

9. An attractive balance of strength and ductility was obtained after solution treatment in the full β condition followed by aging, which converted the α+β microstructure completely to martensite. TiB particles restricted grain growth during β solution treatment, which helped in avoiding ductility reduction.

ACKNOWLEDGEMENT

The present work was supported by the Air Force Office of Scientific Research (AFOSR) under Task 01ML05-COR, and the AFOSR European Office of Aerospace Research and Development (AFOSR/EOARD) within the framework of STCU partner project P-132.

REFERENCES

[1] A.R.G. Brown, H. Brooks, K.S. Jepson, and G.I. Lewis: Technical Note No. MET/PHYS 343, Royal Aircraft Establishment, Farnborough, 1961.

[2] A.E. Palty, H. Margolin, and J.P. Nielsen: *Trans. ASM*, 1954, vol. 46, pp. 312-28.

[3] T.B. Massalski (Ed.): *Binary Alloy Phase Diagrams*, 2 nd ed., ASM International, Materials Park, OH, 1990, p. 547.

[4] S. Tamirisakandala, D.B. Miracle, R. Srinivasan, and J.S. Gunasekera: *Adv Mater. Proc.*, 2006, vol. 164, pp. 41-3.

[5] T.M. Godfrey, P.S. Goodwin, C.M. Ward-Close: *Adv. Eng. Mater.*, 2000; vol. 2, pp.85-92.

[6] D.B. Miracle: in *Metallic Materials with High Structural Efficiency*, O.N. Senkov, D.B. Miracle, and S.A. Firstov (Eds.), Kluwer Academic Publishers, Dordrecht, Netherlands, 2004, pp. 1-18.

[7] C.T. Sims, N.S. Stoloff, and W.G. Hagel: *SUPERALLOYS II*, Wiley-Interscience, New York, NY, 1987.

[8] C. Schuh and D.C. Dunand: *Int. J. Plast.*, 2001, vol. 17, pp. 317-40.

[9] Z. Fan, A.P. Miodovnik, L. Chandrasekaran, and M. Ward-Close: *J. Mater. Sci.,* 1994, vol. 29, pp. 1127-34.

[10] L.V. Artyukh, O.O. Bilous, A.A. Bondar, D.B. Borysov, M.P. Burka, P.S. Martsenyuk, N.I. Tsyganenko, and T.A. Shapoval: *Int. Conf. on Science and Materials in the Frontier of Centuries: Advances and Challenges*, Kyiv, Ukraine, 2002, p. 102

[11] A. Bondar: *Aluminium-Boron-Titanium*, Landolt-Biernstein/New Series, Group IV: Physical Chemistry, vol. 11, Ternary Alloy Systems, Subvolume A, Part 1, Light Metal Systems, G. Effenberg, S. Ilyenko (Eds.,), Springer-Verlag, 2004, pp. 80-101

[12] A.A. Bondar, L.V. Artyukh, O.O. Bilous, T.Ya. Velikanova, S.V. Firstov, D.B. Miracle: in *Int. Conf. on Science and Materials in the Frontier of Centuries: Advances and Challenges*, Kyiv, Ukraine, 2002.

[13] R. Elliott: *Eutectic Solidification Processing. Crystalline and Glassy Alloys*, Butterworth, UK, 1983.

[14] Yu.N. Taran and V.I. Mazur:, Structure of Eutectic Alloys (Structura Evtekticheskih Splavov, in Russ.), Moscow, Metallurgy, 1978.

[15] R.B. Bhat, S. Tamirisa, D.J. Mc Eldowney, D.B. Miracle: in *Materials Science and Technology: Affordable Metal Matrix Composites for High Performance Application II* TMS, Warrendale PA, 2003, pp. 115-24.

[16] O.M. Ivasishin, V.N. Zamkov, P.E. Markovsky, A.N. Kalinyuk, R.V. Teliovich and S.L. Semiatin: in *Ti 2003*, v.2, Wiley-VCH, 2004, pp. 1259-66.

[17] R.V. Teliovich, S.V. Prikhod'ko, S.P. Oshkaderov: *Zavodskaya Laboratoriya*, (in Russian), 1989, vol. 7, p. 45.

[18] R. Boyer, G.E. Welsch, E.W. Collins: *Materials Property Handbook: Titanium Alloys*, ASM International, Materials Park, OH, 1994, pp. 483-636.

[19] S. Tamirisakandala, R.B. Bhat, D.B. Miracle, S. Boddapati, R. Bordia, R. Vanover, and V.K. Vasudevan: *Scripta Mater.*, 2005, vol. 53, pp. 217-22.

[20] O.O. Bilous, L.V. Artyukh, A.A. Bondar, T.Ya. Velikanova, M.P. Burka, M.P. Brodnikovsyi, O.S. Fomichov, N.I. Tsyganenko, S.O. Firstov: *Mater. Sci. Eng. A*, 2005, vol. 402A, pp. 76-83.

[21] V.G. Lazarev, T.K. Polyakova: *Non-Ferrous Metals* (Zvetnye Metally, in Rus.), No 3, 1982, pp. 86-87.

[22] S. Gorsse and D.B. Miracle: *Acta Mater.*, 2003, vol. 51, pp.2427-42.

[23] C.F. Yolton, and J.H. Moll: *Titanium'95: Science and Technology,* P.A. Blenkinsop, W.J. Evans, H.M. Flower (Eds.), The Institute of Materials, London, UK, 1996, pp. 2755-62.

[24] Z. Fan, L. Chandrasekaran, C.M. Ward-Close, and A.P. Miodovnik: *Scripta Metall. Mater.*, 1995, vol. 32, pp. 833-838.

[25] *Metallic Materials Properties Development and Standardization (MMPDS)*, Scientific Report, National Technical Information Service (NTIS), Springfield, Virginia, January 2003.

[26] S. Tamirisakandala, R.B. Bhat, D.J. McEldowney, and D.B. Miracle: *Materials Science and Technology: Affordable Metal Matrix Composites for High Performance Applications II*, 2003, TMS, Warrendale, PA, pp. 185-94.

[27] O. M. Ivasishin and R. V. Teliovich: *Mat. Sci. Eng.*, 1999, vol. A263, pp. 142-54.

Table 1 Chemical compositions (in weight percent) of the materials in this study.

Ingot ID	Al	V	B	O	N	Ti
Ti	<0.05	<0.05	<0.05	0.034	0.009	bal.
TiB	<0.05	<0.05	18.2	0.08	0.01	bal.
AlB_2	55.4	<0.05	44.4	0.15	0.04	
Al-40V	59.5	39.3	<0.05	0.12	0.03	
1-1	5.9	4.05	<0.05	0.08	0.02	bal.
1-2	5.85	4.1	0.5	0.07	0.03	bal.
1-3	5.9	4.0	1.4	0.07	0.03	bal.
1-4	6.1	4.0	1.5	0.08	0.02	bal.
1-5	6.0	4.0	1.55	0.07	0.03	bal.
1-6	6.05	3.95	1.6	0.08	0.03	bal.
1-7	6.05	4.00	1.85	0.08	0.03	bal.
2-1	5.80	4.00	1.50	0.09	0.04	bal.
2-2	5.90	3.90	1.55	0.09	0.04	bal.
2-3	5.80	3.90	1.55	0.10	0.04	bal.
3-1	5.70	3.90	1.50	0.12	0.07	bal.
3-2	5.80	3.90	1.55	0.13	0.07	bal.
3-3	5.80	3.90	1.50	0.12	0.07	bal.

Table 2 Tensile Properties of Ti64-1.55B compared with Ti64.

Alloy	Condition	Tensile Property				
		Elastic modulus, GPa	YS, MPa	UTS, MPa	Elong., %	RA, %
Ti64	As-cast [25]	116	827	861	5	
	Forged [25]	116	882	950	10	25
	Extruded + MA [25]	116	854	944	10	20
	Extruded + STA [25]	116	1012	1123	6	12
Ti64-1.55B	As-cast (random)	134	fracture below YS			
	As-cast (aligned)	138* 127**	999	1033	0.9	5
	3D-Forged	132	1065	1128	2.7	8
	3D-Forged + Rolled	142*	1170	1230	6.0	21
	3D-Forged + Rolled + beta-STA	148*	1380	1495	4.6	15
	As-cast + Direct β Rolling	145*	1216	1368	4.7	25
	As-cast+Direct β Extrusion*		1185	1200	4.9	16

* longitudinal direction
** transverse direction

LIST OF FIGURE CAPTIONS

Fig. 1 Titanium rich end of the binary Ti-B phase diagram (from [3]).

Fig. 2 Schematic of vacuum arc-induction furnace with independent control of arc power (W_1), induction power (W_2), and withdrawal rate (R) used to vary the melt pool size and shape: (a) W_1 = 9 kWA, W_2 =40 kWA, R = 0.05 mm s^{-1}; (b) W_1 = 6 kWA, W_2 =50 kWA, R = 0.03 mm s^{-1}. Isotherms are normal to the thermal gradients and are shown schematically in the two lower pictograms.

Fig. 3 Schematic of the thermo-mechanical processing sequence used to process 70 mm diameter ingots.

Fig. 4 Isopleths calculated for Ti64-B system: (a) Ti64-B using PANDAT, (b) Ti64-0.18O-TiB using PANDAT, and (c) Ti64-B using ThermoCalc [9].

Fig. 5 Secondary electron micrographs obtained on deep etched specimens of (a) Ti64-1.4B (hypoeutectic) and (b) Ti64-1.67B (hypereutectic).

Fig. 6 DTA cooling curves for (a) Ti64-1.5B, (b) Ti64-1.55B, and (c) Ti64-1.6B.

Fig. 7 Microstructures of as-cast Ti64-1.55B cooled at different rates: (a) 0.2 Ks^{-1}, (b) 0.7 Ks^{-1}, (c) 1.3 Ks^{-1}, (d) 2.7 Ks^{-1}, (e) >50 Ks^{-1}, and (f) >300 Ks^{-1}. Micrographs (a)-(e) are optical images and micrograph (f) is secondary electron image obtained on a deep-etched specimen.

Fig. 8 Micrographs at various locations of the 70 mm diameter ingot illustrating the influence of cooling rate on the eutectic microstructure. Micrographs (a)-(c) are secondary electron images on deep etched specimens and (d)-(g) are optical images.

Fig. 9 Optical micrographs illustrating two types of cast eutectic microstructures: (a) aligned TiB and (b) random TiB.

Fig. 10 Pole figures of as-cast aligned microstructure: (a) (100) α-Ti and (b) (020) TiB.

Fig. 11 Modelling of eutectic texture: (a) Δ, 0, □ – poles of {111}, {011} and {100} respectively of initial β-phase single crystal. ■ – theoretical poles of (100), (010) and (110) α-phase for 4 variants of Burgers orientation relationship; Δ, 0, □ – poles of

{111}, {011} and {100} respectively of initial β-phase single crystal. ■ – theoretical poles of (100), (010) and (110) α-phase for 3 variants of Burgers orientation relationship. (a) $<100>_{\beta}$ axial texture with 4 Burgers OR variants and (b) $<111>_{\beta}$ axial texture with 3 Burgers OR variants.

Fig. 12 Heating curves obtained from DTA on Ti64 with 0.5B, 1.55B, and 1.65B at a heating rate of 40 Ks^{-1}.

Fig. 13 Heating curves obtained from DTA on Ti64-1.4B for a heating rate of 20 Ks^{-1} and 80 Ks^{-1}.

Fig. 14 (a) Calculated dependencies of Al and B content in Ti matrix on B concentration in Ti-64. Data points represent the experimentally measured values on the Ti64-1.5B, (b) calculated (solid line) and experimentally measured β transus values of Ti64 as a function of B concentration.

Fig. 15 Optical micrographs of Ti64-1.55B after thermo-mechanical processing: (a) after 3D forging, (b) after slab forming, and (c) after 1D rolling (rolling direction is vertical).

Fig. 16 Optical micrographs of Ti64-1.55B (a) after direct 1D rolling and (b) heavily fragmented TiB plates in the starting as-cast condition.

Fig. 17 Backscattered electron images of Ti64-1.55B after direct extrusion (a) longitudinal and (b) transverse. The extrusion direction in micrograph (a) is horizontal.

Fig. 18 Fracture surfaces of tensile specimens of as-cast Ti64-1.55B (a-b) random TiB and (c) aligned TiB.

Fig. 19 Fracture surfaces of tensile specimens of Ti64-1.55B after thermo-mechanically processing (a-b) after 3D forging and (c-d) after 1-D rolling.

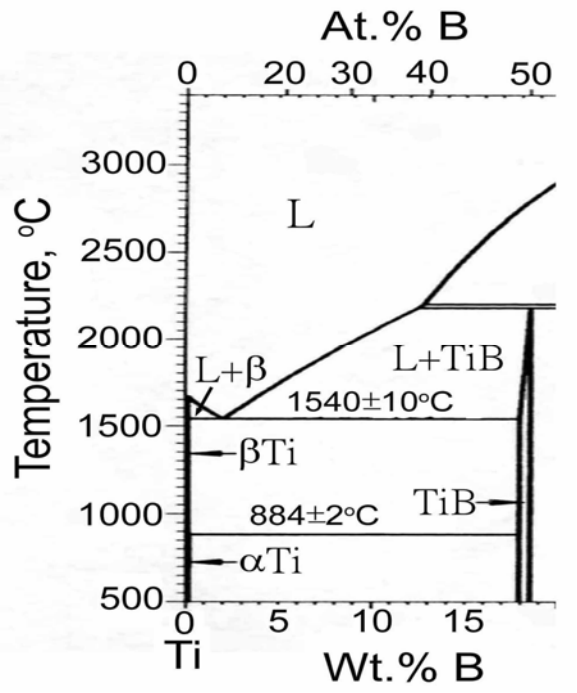
At.% B
0
20
30
40
50
3000
2500
2000
1500
1000
500
Temperature, °C
L
L+β
L+TiB
1540±10°C
βTi
TiB
884±2°C
αTi
0
5
10
15
Ti
Wt.% B

Fig.1

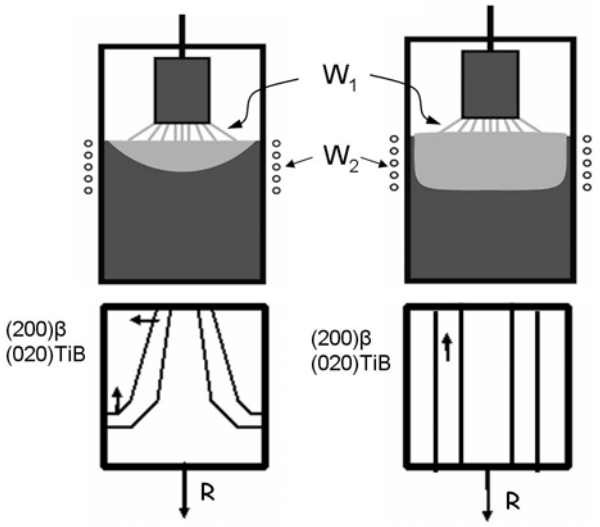
W1
W2
(200)β
(020)TiB
R
(200)β
(020)TiB
R

Fig.2

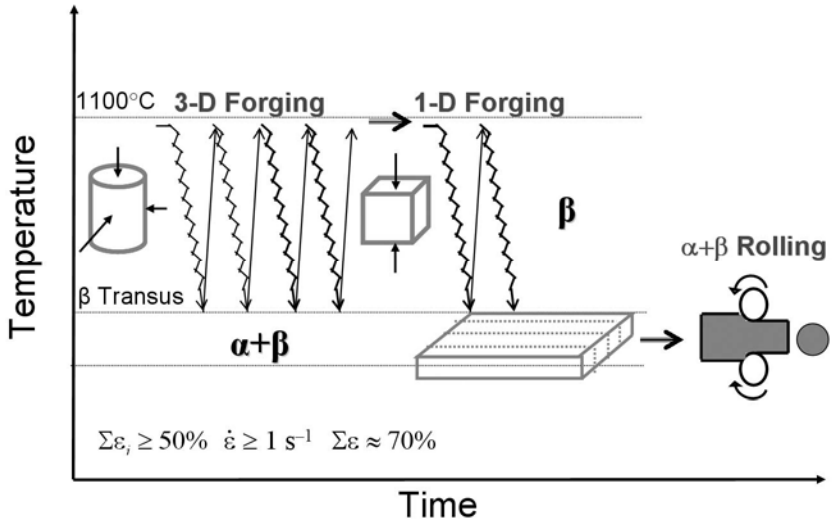
1100°C
3-D Forging
1-D Forging
β
α+β Rolling
β Transus
α+β
Temperature
Time
$\Sigma\varepsilon_i \geq 50\%$ $\dot{\varepsilon} \geq 1\ s^{-1}$ $\Sigma\varepsilon \approx 70\%$

Fig. 3

(a)

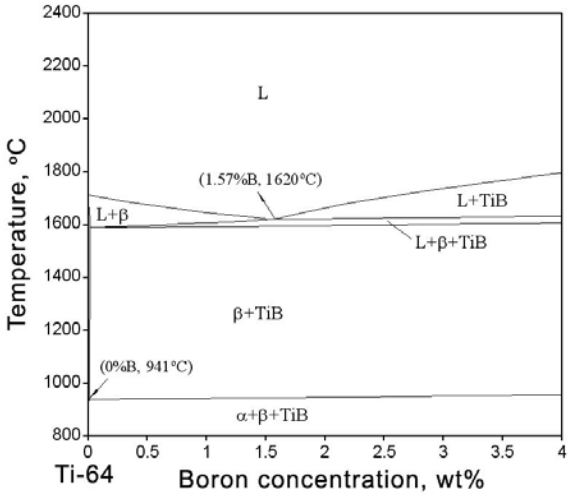
L
(1.57%B, 1620°C)
L+TiB
L+β
L+β+TiB
β+TiB
(0%B, 941°C)
α+β+TiB
Temperature, °C
Ti-64
Boron concentration, wt%

(b)

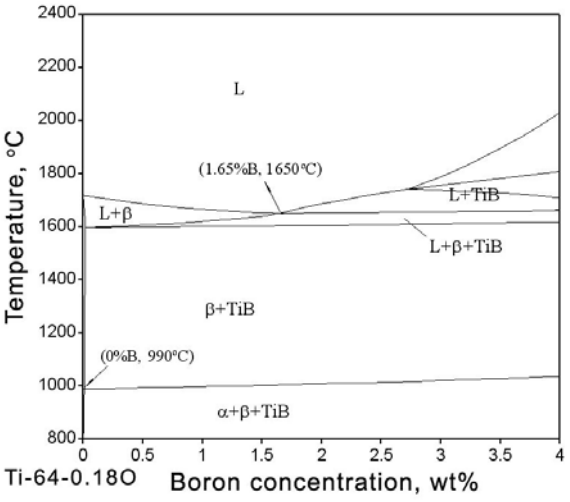
L
(1.65%B, 1650°C)
L+TiB
L+β
L+β+TiB
β+TiB
(0%B, 990°C)
α+β+TiB
Temperature, °C
Ti-64-0.18O
Boron concentration, wt%

(c)

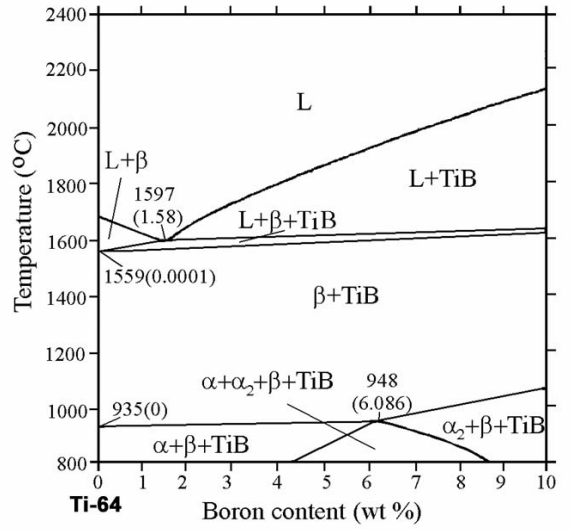
L
L+β
1597
(1.58)
L+TiB
L+β+TiB
1559(0.0001)
β+TiB
α+α2+β+TiB
948
(6.086)
935(0)
α2+β+TiB
α+β+TiB
Temperature (°C)
Ti-64
Boron content (wt %)

Fig. 4

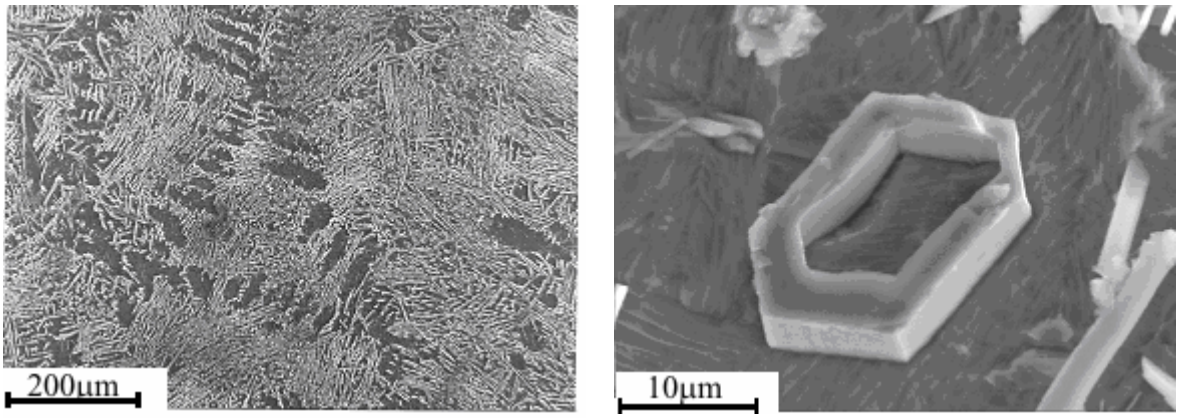
200μm
10μm

(a) (b)

Fig. 5

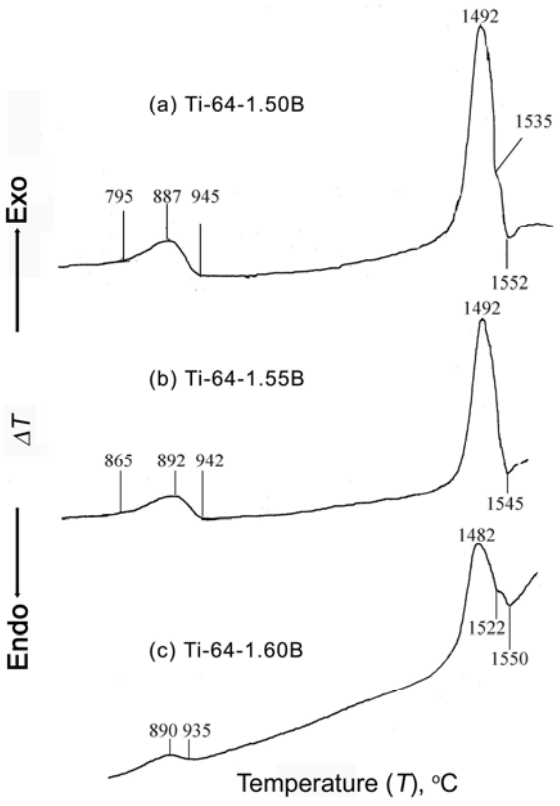
(a) Ti-64-1.50B
1492
1535
795
887
945
1552
(b) Ti-64-1.55B
1492
865
892
942
1545
(c) Ti-64-1.60B
1482
1522
1550
890
935
Exo
Endo
ΔT
Temperature (T), °C

Fig 6

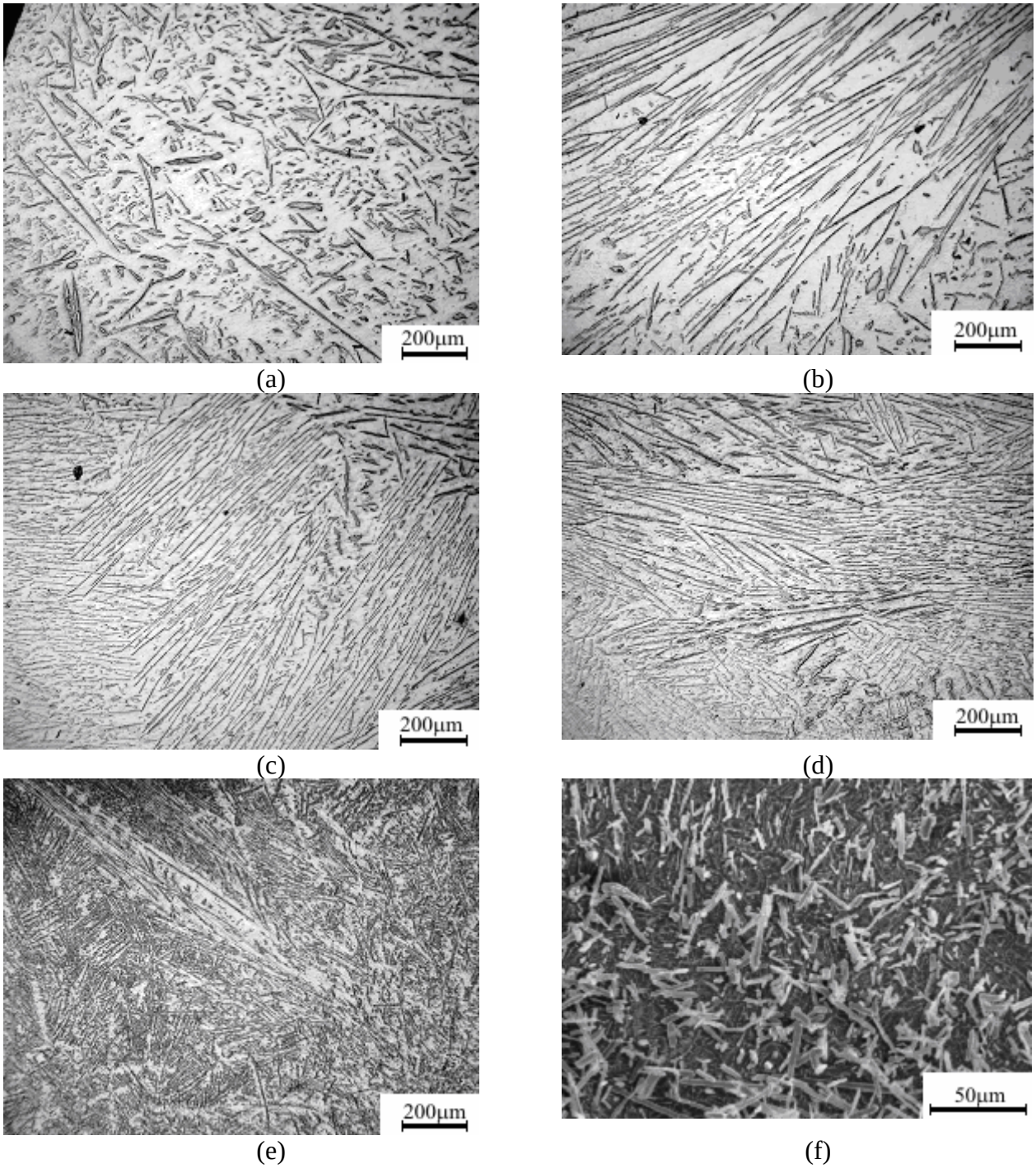

Fig. 7

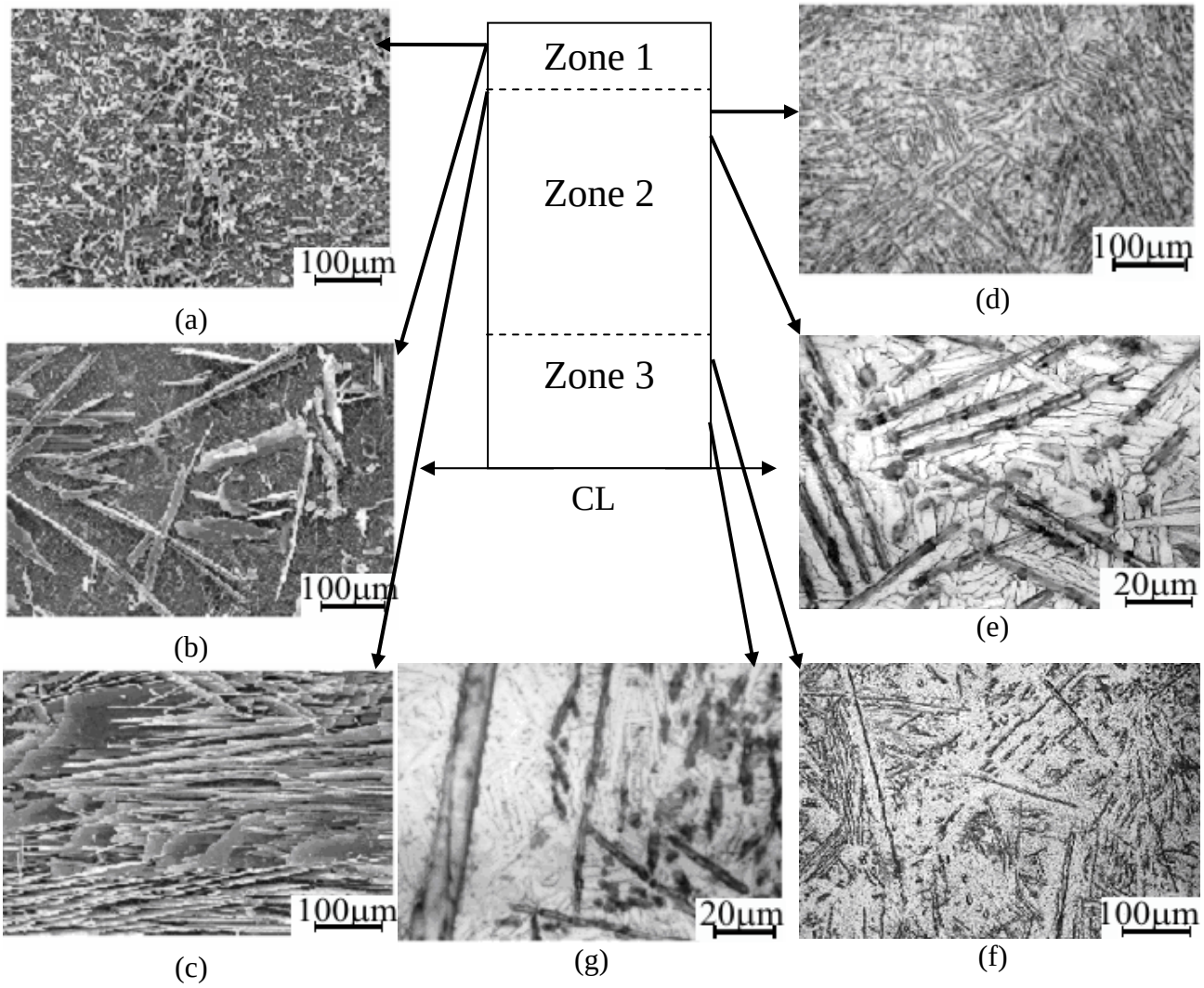
Zone 1
Zone 2
Zone 3
CL
100μm
(a)
100μm
(b)
100μm
(c)
20μm
(g)
100μm
(d)
20μm
(e)
100μm
(f)

Fig.8

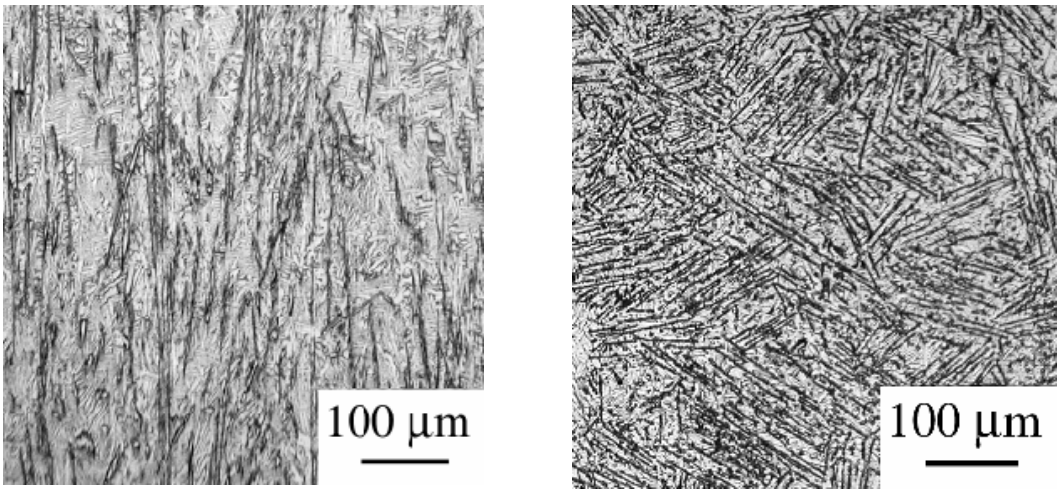

(a) (b)

Fig. 9

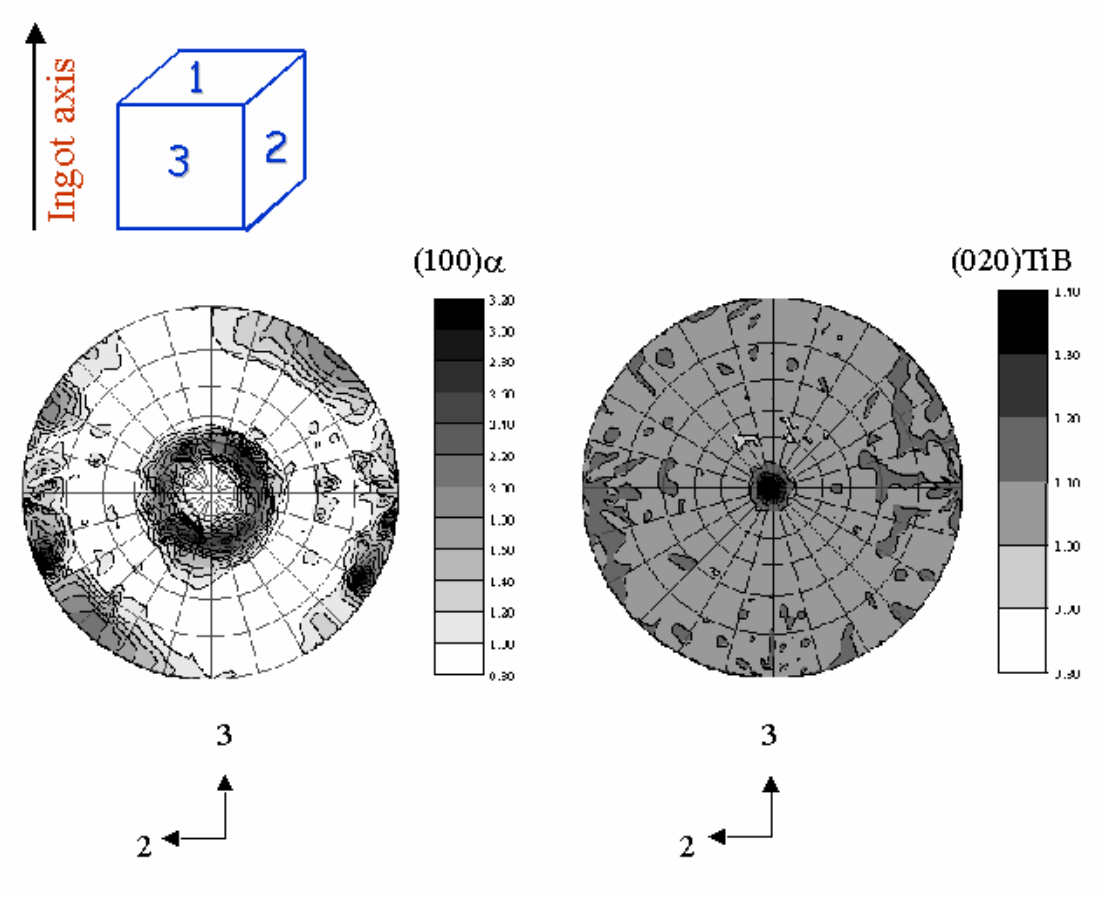

(a) (b)

Fig. 10

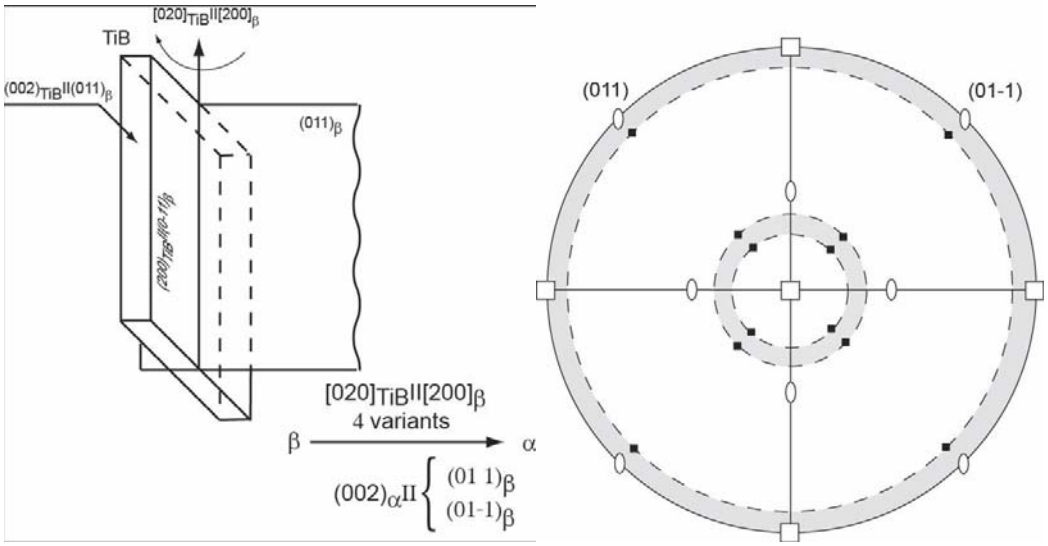
TiB
[020]TiBII[200]β
(002)TiBII(011)β
(011)β
[020]TiBII[200]β
4 variants
β
α
(002)αII
(01 1)β
(01-1)β
(011)
(01-1)

(a)

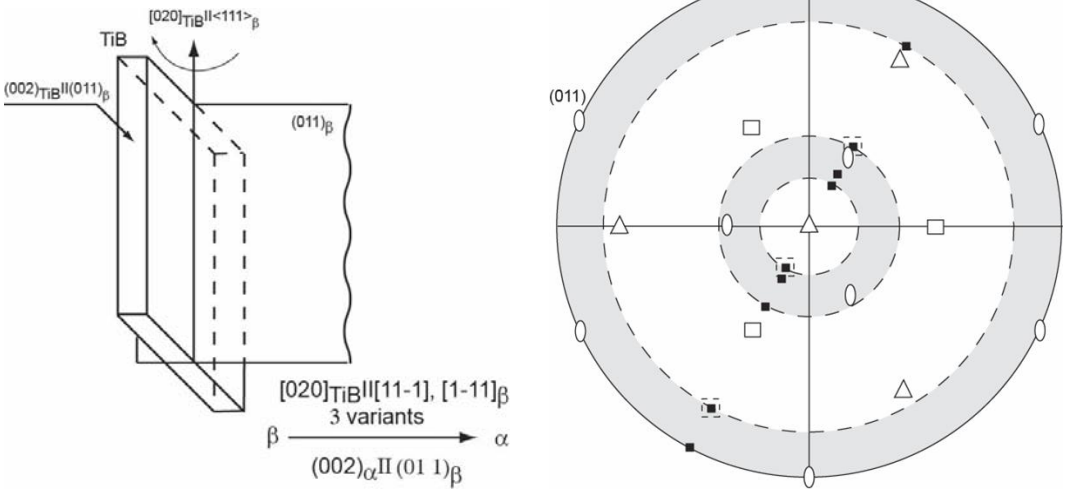
TiB
[020]TiBII<111>β
(002)TiBII(011)β
(011)β
[020]TiBII[11-1], [1-11]β
3 variants
β
α
(002)αII (01 1)β
(011)

(b)

Fig. 11

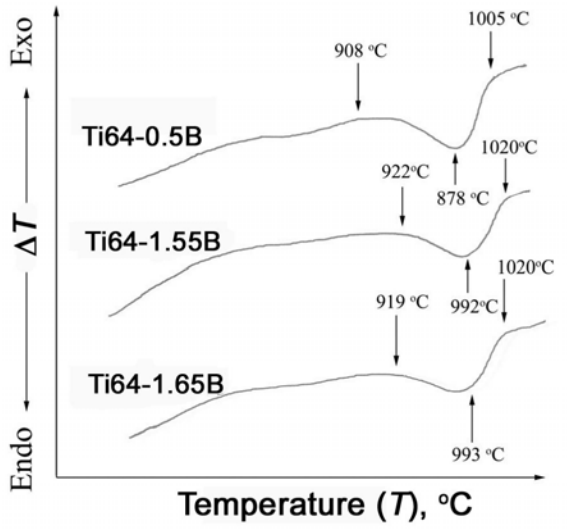
Exo
ΔT
Endo
Ti64-0.5B
908 °C
1005 °C
1020°C
922°C
878 °C
Ti64-1.55B
1020°C
919 °C
992°C
Ti64-1.65B
993 °C
Temperature (T), °C

Fig. 12

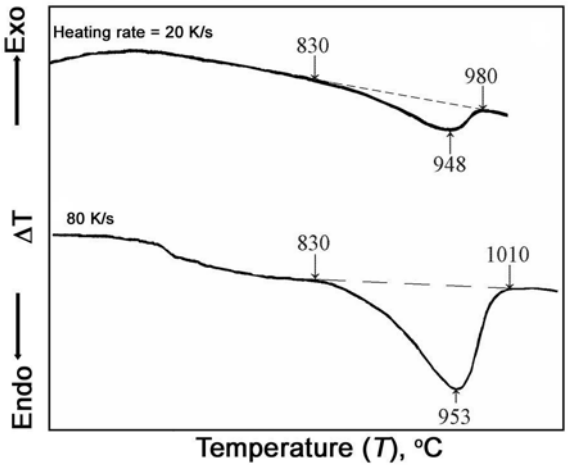
Exo
Heating rate = 20 K/s
830
980
948
ΔT
80 K/s
830
1010
Endo
953
Temperature (T), °C

Fig. 13

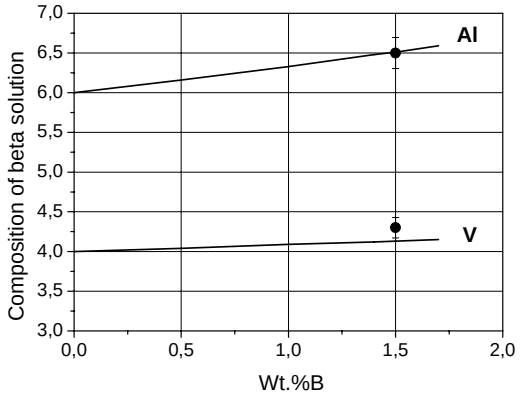
Composition of beta solution
Wt.%B
Al
V
7,0
6,5
6,0
5,5
5,0
4,5
4,0
3,5
3,0
0,0
0,5
1,0
1,5
2,0

(a)

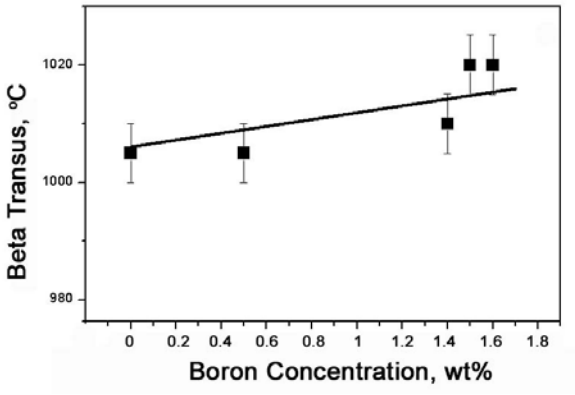
Beta Transus, °C
Boron Concentration, wt%
1020
1000
980
0
0.2
0.4
0.6
0.8
1
1.2
1.4
1.6
1.8

(b)

Fig. 14

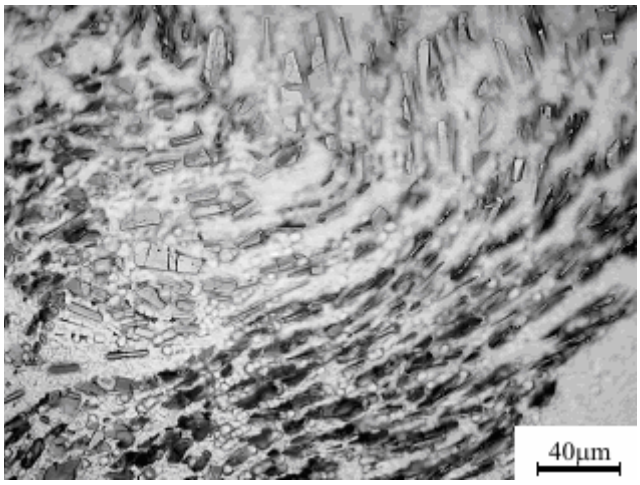

(a)

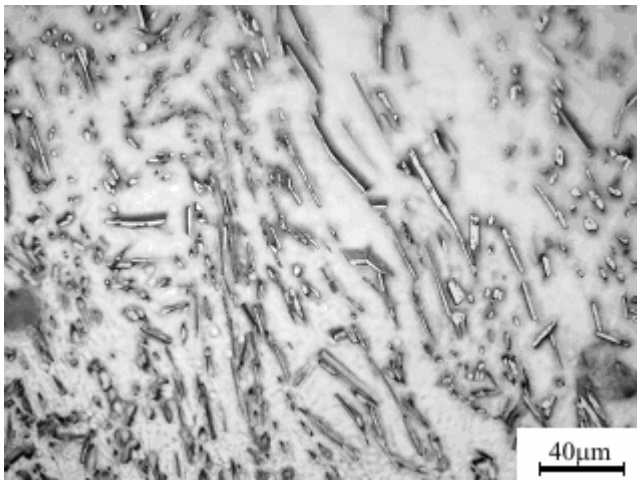

(b)

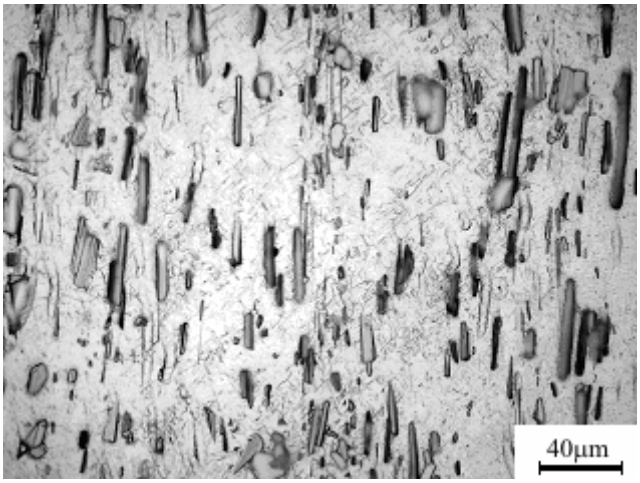

(c)

Fig. 15

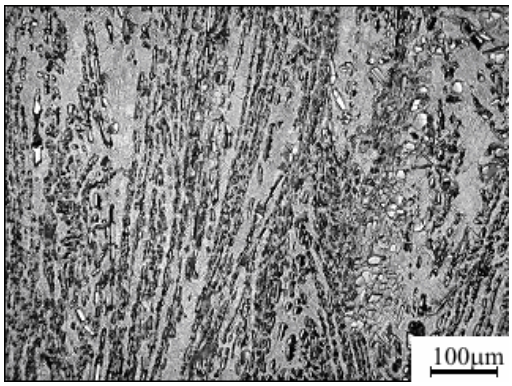

(a)

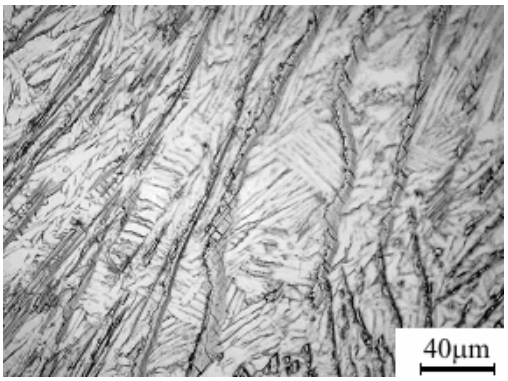

(b)

Fig. 16

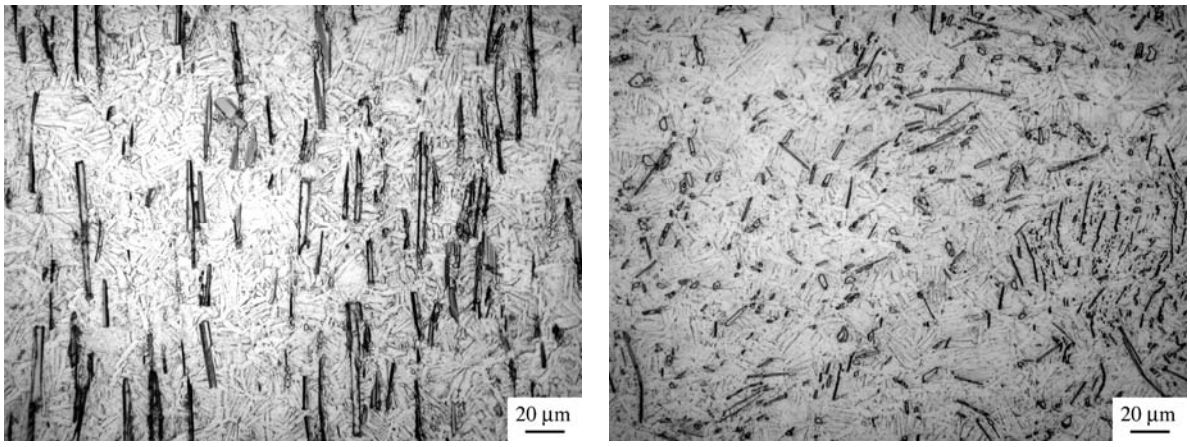

(a) (b)

Fig. 17

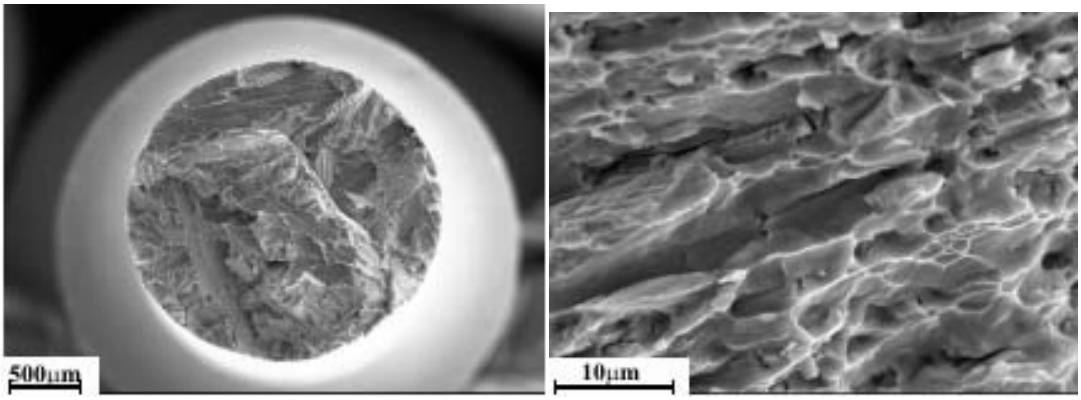

(a) (b)

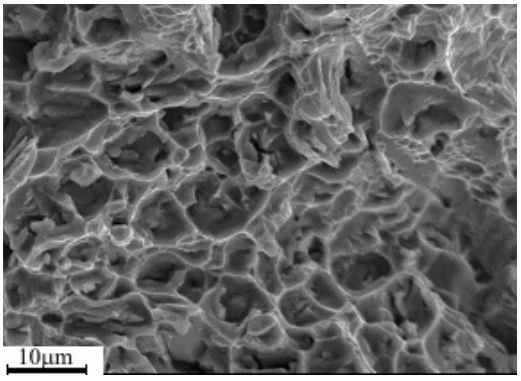

(c)

Fig. 18

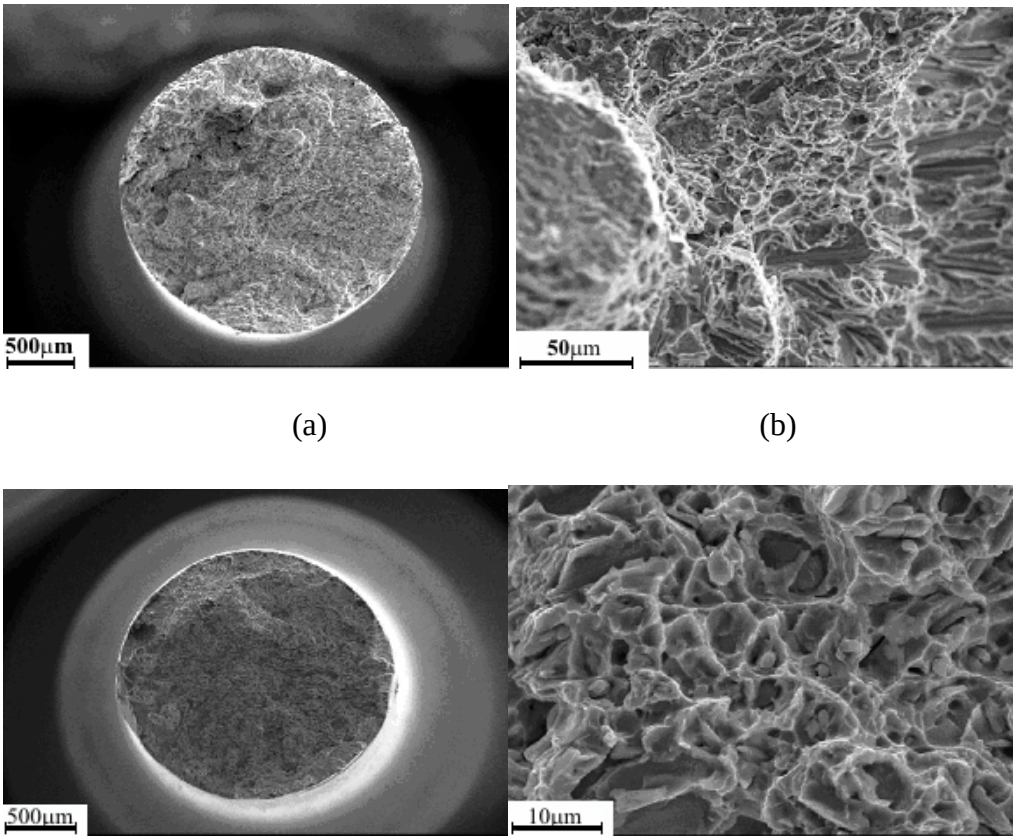

Fig. 19